REVIEW

Graphene-Based Materials for Lithium-Ion Hybrid Supercapacitors

Yanfeng Ma, Huicong Chang, Miao Zhang, and Yongsheng Chen*

Lithium-ion hybrid supercapacitors (LIHSs), also called Li-ion capacitors, have attracted much attention due to the combination of the rapid charge–discharge and long cycle life of supercapacitors and the high energy-storage capacity of lithium-ion batteries. Thus, LIHSs are expected to become the ultimate power source for hybrid and all-electric vehicles in the near future. As an electrode material, graphene has many advantages, including high surface area and porous structure, high electric conductivity, and high chemical and thermal stability, etc. Compared with other electrode materials, such as activated carbon, graphite, and metal oxides, graphene-based materials with 3D open frameworks show higher effective specific surface area, better control of channels, and higher conductivity, which make them better candidates for LIHS applications. Here, the latest advances in electrode materials for LIHSs are briefly summarized, with an emphasis on graphene-based electrode materials (including 3D graphene networks) for LIHS applications. An outlook is also presented to highlight some future directions.

1. Introduction

Driven by the ever-increasing demand of modern society for portable electronic devices, renewable energy products, and electric or hybrid electric vehicles, research on environmentally friendly energy-storage devices with high-performance and low-cost has been dramatically expanded. Supercapacitors (electrochemical capacitors) and Li-ion batteries (LIBs) are currently the two most-promising energy-storage devices.[1–5] Supercapacitors have a high power density (10 kW kg^{-1}) and long cycle life but suffer from low energy density (only 5–10 W h kg^{-1}). On the other

hand, lithium-ion batteries can provide high energy densities (150–200 W h kg^{-1}), but their power densities are relatively low (below 1 kW kg^{-1}) and their cycle life is quite poor (usually less than 1000 cycles). However, in the view of applications in electronic devices and hybrid electric vehicles, energy-storage devices with both high energy and power density are demanded urgently. To solve this problem, one way is to fabricate new electrode materials with high electrochemical performance, and the other is to design hybrid energy-storage devices that possess both high energy and power density.[6] Lithium-ion hybrid supercapacitors (LIHSs) have emerged as such a solution.[6–14]

Lithium-ion hybrid supercapacitors (LiHSs), also known as Li-ion capacitors (LICs), are constructed from a capacitor-type electrode and a lithium-ion-battery-type electrode with a Li-salt-containing electrolyte. These two electrodes operate reversibly in different potential ranges, thus increasing the operation voltage and providing an opportunity to achieve fast charge capability, robust cycle life and high energy density. The challenge to fabricate such a high-performance hybrid supercapacitor is to couple appropriately both high-performance capacitor-type and battery-type electrode materials in the devices. Currently, the commonly used capacitor-type electrode materials are carbonaceous materials (activated carbon (AC), carbon nanotube, graphene etc.), and the battery-type electrode materials used are insertion-type materials including carbonaceous materials, metal oxides and hydroxides, and intercalation compounds and their composites. Among the carbonaceous materials, activated carbon is the most widely used due to its high surface area and relatively low cost.[11,13] In early 2000, a LIHS system, which was constructed from a graphite cathode and an activated carbon anode, was commercialized as "the generation-II supercapacitors",[7] with a cell voltage of 3.8 V and a specific energy of 20 W h kg^{-1}, much higher than practical AC-based supercapacitors, and a power density up to 3 kW kg^{-1}, 3-fold higher than of commercial LIBs (below 1 kW kg^{-1}). However, the large number of small pores (<0.8 nm) in ACs, which prevents the migration of electrolyte ions, and the relatively low electric conductivity restrict its electrochemical performance.[12] Compared with AC, graphene has a higher electric conductivity and a more-flexible pore structure, which makes it a good candidate for next-generation energy-storage devices.[15,16] Though bulk graphene materials suffer from restacking, construction of

Prof. Y. Ma, Dr. H. Chang, Dr. M. Zhang,
Prof. Y. Chen
The Key Laboratory of Functional Polymer
Material and Centre for Nanoscale
Science and Technology
Institute of Polymer Chemistry
College of Chemistry
Nankai University
Tianjin 300071, China
E-mail: yschen99@nankai.edu.cn
Prof. Y. Ma, Dr. H. Chang, Dr. M. Zhang,
Prof. Y. Chen
Collaborative Innovation Center of
Chemical Science and Engineering
Nankai University
Tianjin 300071, China

3D crosslinked graphene bulk material (3D graphene) can highly improve this problem.[17–19] Thus, graphene-based 3D materials are promising electrode materials for LiHS applications.

There have been several special reviews on LIHSs.[6–9] Dubal et al.[6] described the roadmap to hybrid materials and devices aiming at enhancing the electrochemical performance of energy systems. Naoi et al.[7] compared LIHSs with electrochemical double-layer capacitors (EDLCs), and then put emphasis on nanohybrid capacitors. Aravindan et al.[8] summarized the insertion-type electrodes for non-aqueous LIHSs in detail. Wang et al.[9] summarized the electrode materials for aqueous asymmetric supercapacitors. Also, some reviews of energy-storage systems have mentioned the progress in Li-ion capacitors.[1,4,10–13] However, so far, graphene-based LiHSs have not been systematically presented. Thus, in this review, we will briefly summarize the latest advances in electrode materials for LiHSs, especially the graphene-based materials for LIHS applications, either as positive- or as negative-electrode materials. Also, in view of the latest development of 3D graphene,[17,18] which exhibits many unique properties, we will address some of the research effort on this material. Finally, an outlook will be presented to highlight some future directions.

2. Lithium-Ion Hybrid Supercapacitors (LiHSs)

2.1. Basis of LiHSs

LiHSs are constructed from an electrochemical capacitor-type electrode and a Li-ion-battery-type electrode with a lithium-ion-containing electrolyte. Based on the different energy-storage mechanisms, supercapacitors can be classified into electrochemical double-layer capacitors (EDLCs) and pseudocapacitors (PCs).[2] In EDLCs, the energy is physically stored through the adsorption of ions on the surface of the electrodes. Porous carbon materials such as activated carbon, carbon nanotubes, and graphene are the commonly used active materials for electrodes. Pseudocapacitors store energy through the fast surface redox reactions occurring between the active materials in the electrode and the electrolyte. Metal oxides and conducting polymers are the most extensively explored electrode materials. A lithium-ion battery is a rechargeable battery in which Li^+ ions move from the negative electrode to the positive electrode during discharge and back when charging. In LIBs, the commonly used lithium-releasing cathode is a layered lithium metal oxide, and the lithium-accepting anode materials are graphite and graphene. LiHSs are usually constructed from an EDLC-type electrode (high specific surface area (SSA) carbonaceous materials) and an LIB-type electrode (insertion-type materials).

Unlike EDLCs and PCs, which have a symmetric cell configuration, LIHSs are a type of asymmetric supercapacitor (**Figure 1**).[20] EDLCs adopt a non-Faradaic, double-layer charge–discharge mechanism (Figure 1a). LIHSs work with anions adsorbing/desorbing onto/from the positive electrode surface and Li^+ ions intercalating/de-intercalating into/from the bulk of the negative electrode simultaneously.[1] The combination of the Faradaic intercalation and non-Faradaic surface reaction provides an opportunity to improve both the energy and power density simultaneously.

Yanfeng Ma received her B.S. (1994) in Physical Chemistry and Ph.D. (2003) in Physical Chemistry from Nankai University. Since 2003, she has been an Associate Professor of Chemistry at Nankai University. Her research interests focus on controlled synthesis and application of carbon nanomaterials (graphene and carbon nanotubes), carbon-based functional materials, nanocomposites, and nanodevices.

Huicong Chang received her BE degree from the polymer material and engineering department of Hebei University, China in 2012. She is currently studying for a doctoral degree in Yongsheng Chen's group. Her research interests include the synthesis and application of graphene and graphene-based materials.
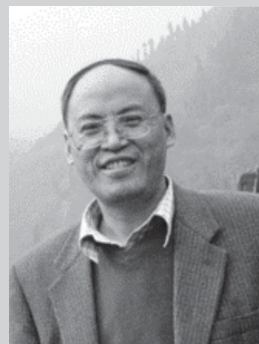
Yongsheng Chen graduated from the University of Victoria with a Ph.D. degree in chemistry in 1997 and then joined the University of Kentucky and the University of California at Los Angeles for postdoctoral studies from 1997 to 1999. From 2003, he has been a Chair Professor at Nankai University. His main research interests include: i) carbon-based nanomaterials, including carbon nanotubes and graphene; ii) organic and polymeric functional materials, and iii) energy devices including organic photovoltaics and supercapacitors.

The energy (E in W h kg^{-1}) and power density (P in W kg^{-1}) of the device can be expressed as $E = \frac{1}{2}CV^2$ and $P = V^2/4R$, respectively.[1] In the equations, C (in F) is the total capacitance of the cell; V (in V) is the cell's operating voltage; and R is the equivalent series resistance (ESR) (in Ω). It is noteworthy that both the energy and power densities are proportional to the square of the operating voltage. Increasing the operating voltage is of critical significance for improving both the energy and power densities. In LIHSs, the two electrodes operate reversibly in different potential ranges with different electrochemical mechanisms; thus, a higher operation voltage can be achieved, and hence both the energy
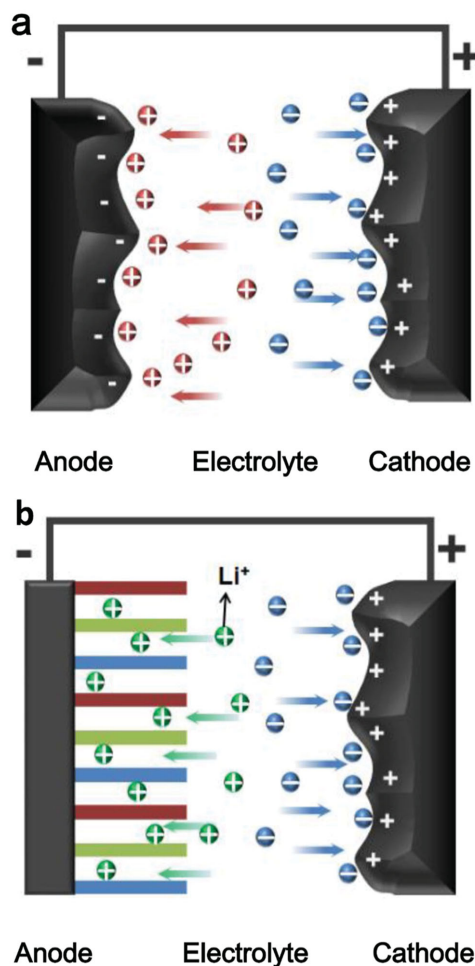
Figure 1. Electrochemical reaction mechanism of a) EDLCs and b) LIHSs. Reproduced with permission.[20] Copyright 2014, Wiley.

Figure 2. Typical voltage profiles for an EDLC cell and an LIHS cell. The EDLC cell utilizes activated carbon for both its positive and negative electrodes. The LIHS cell uses activated carbon for the positive electrode and graphite for the negative electrode. For the operation of the LIHS cells, the negative graphite electrode must be pre-lithiated. Reproduced with permission.[7] Copyright 2012, The Royal Society of Chemistry.

and power density can be greatly improved. **Figure 2** exhibits the typical voltage profiles for a commercial EDLC cell and a practical LIHS cell that utilizes activated carbon for the positive electrode and graphite for the negative electrode. The maximum voltage of a commercial EDLC with activated carbon for both electrodes is limited to 2.7 V when organic electrolyte systems such as acetonitrile are used; exceeding this voltage limitation will cause serious damage to the EDLC cell and considerable side reactions.[7] LIHSs can achieve a high voltage of over 4.0 V, and thus the energy density can be enhanced more than threefold over EDLCs.[7]

The operating voltage also can be elevated by use of electrolytes with a large operating voltage. From this point of view, organic electrolytes (2.5–3.0 V) and ionic liquids (up to 4 V) are more attractive than aqueous electrolytes (1.0–1.5 V).

Another important factor for the energy density is the specific capacitance. The specific capacitance has been found to be mainly affected by such factors as the SSA and pore-size distribution (PSD) of the active electrode material, the electric conductivity of both the active material and the electrolyte, and the extra redox capacitance of the electrode materials.[1] However, for the high-surface-area materials used for supercapacitor applications, a linear correlation between the total SSA and the capacitance performance has not been found. In fact, the effective SSA (E-SSA) that is accessible by the electrolyte ions has been observed to be directly correlated with the specific capacitance.[21] The E-SSA is defined as the cumulative density functional theory (DFT) SSA of pores with a size above the ion diameter of different electrolytes. Thus, for carbonaceous materials, effective approaches to enhance the energy density include designing and fabricating nanoporous structures to obtain a high E-SSA, introducing pseudocapacitive species including heteroatom doping to obtain extra redox capacitance, etc. For pseudocapacitive materials like metal oxides, a convenient way is to construct composites with nanostructured carbon materials, which serve as supports to supply a high E-SSA and improve the conductivity. As to the conductivity of the electrolyte, aqueous electrolytes are more conductive than non-aqueous ones.

For the power density, another important factor is the electron spin resonance (ESR), which is determined by the conductivity of the electrode materials and the electrolytes, the contact resistance between the electrode materials and the current collector, and both the diffusion distance and rate of ions in the electrode materials.[1] Therefore, improving of the E-SSA and conductivity of the electrode material and using an aqueous electrolyte will decrease the ESR and favor the improvement of the power density.

In general, when the electrolyte is determined, the effective approach to obtain both a high energy and power density is to improve the effective SSA and conductivity of the electrode materials and couple appropriate positive- and negative-electrode materials.

2.2. Electrolytes

Electrolytes can be aqueous or non-aqueous (organic). Aqueous electrolytes have low viscosity and therefore have high mobility. The main disadvantage is they can only sustain a voltage up
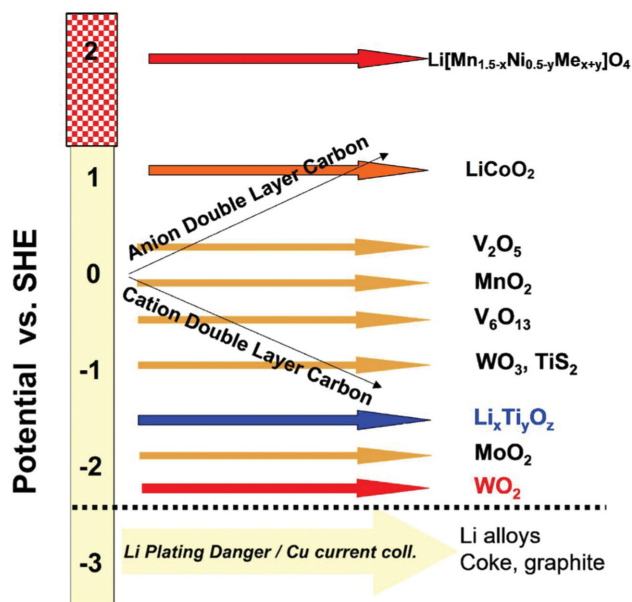
Figure 3. Schematic illustration of the relative potentials of the positive and negative electrodes of EDLCs based on AC as a function of charge, and the general redox potential of various intercalation compounds. Reproduced with permission.[22] Copyright 2006, Springer.

to 1 V.[11] In contrast, non-aqueous electrolytes can sustain a high voltage up to 3 V; however, they have high viscosity and therefore low ionic conductivity.

The commonly used aqueous electrolytes are alkaline sulfates (X_2SO_4 aq.), hydrates (XOH aq.), or nitrates (XNO_3 aq.), where X = Li, Na, or K with concentration ranges of 0.1–6 M.[7] Aqueous LIHSs show higher specific power because aqueous electrolytes have a high ionic conductivity compared with those of non-aqueous ones. However, these LIHS systems have low specific energy because of their low operating voltage, which results from the narrow electrochemical window of the aqueous electrolytes.

As non-aqueous LIHS systems have considerably higher energy density compared with aqueous systems, because they can offer a wider electrochemical window, they have been widely investigated and used in most commercial products.[1,6] However, the low ionic conductivity and large anion size limit the power density. In non-aqueous LIHS systems, the most commonly used electrolyte is $LiPF_6$ in an organic solvent (ethylene carbonate (EC) and dimethyl carbonate (DMC)).

2.3. Electrode Materials

The commonly used electrode materials in LIHS systems include carbonaceous materials, metal oxides and hydroxides, and intercalation compounds. The challenge to fabricate high-performance LIHSs is to couple appropriate positive- and negative-electrode materials in the devices. Taking AC as an example. it can be used as either a positive or a negative electrode, depending on the relative potentials of the counter electrodes. **Figure 3** shows the relative potentials of the positive and negative electrodes of an EDLC based on AC as a function of

charge and the general redox potential of various intercalation compounds.[22] When AC is used as the positive electrode, two extreme cases are V_2O_5 and graphite. The use of V_2O_5 as the negative material will make the initial voltage of the cell negative, while graphite materials would result in a cell with the highest voltage. According to ref.,[22] the ideal potential of Li intercalation is dictated by the electrochemical window between the lithium titanates and the WO_2.

Another noteworthy point is the mass ratio between the positive and negative electrodes. An appropriate mass balance certainly leads to a substantial increase in both the net operating potential and energy density.[8] The following equation has been used to calculate the optimized mass ratio between the positive and negative electrodes, according to a charge balance between the positive and negative electrodes:[1]

$$\frac{m_+}{m_-} = \frac{C_- \Delta E_-}{C_+ \Delta E_+} \tag{1}$$

where m, C, and ΔE are the electrode mass and specific capacitance, and the potential range in the charge/discharge process for both electrodes, respectively.

In aqueous LIHS systems, several metal oxides, such as NiO,[23–25] MnO_2,[26] V_2O_5,[27] and Fe_3O_4,[28] have been used as positive electrode materials in combination with activated carbon (AC) as the negative electrode. Among these metal oxides, MnO_2 has some advantages in terms of high specific capacity (1370 F g^{-1}), low cost, natural abundance, high safety, ease of preparation, and non-toxicity, and thus has been the most studied.[1,6–8] Yuan et al.[26] reported the fabrication of nanoneedles (20–100 nm) of a MnO_2/carbon composite (g-MnO_2) via solid-state grinding. By using of this g-MnO_2 as the positive-electrode material and AC as the negative, the hybrid supercapacitor presented the reported highest energy density of 50 W h kg^{-1} for an aqueous system. Other metal-oxides-based hybrid-supercapacitor aqueous systems generally gave lower energy densities (15–30 W h kg^{-1}).[7]

In non-aqueous LIHS systems, the positive electrode materials are usually AC,[13] oxides, hydroxides, and polyanions.[8] Apart from AC, $Li_4Ti_5O_{12}$ (LTO) and other crystal forms of Ti oxides exhibit favorable properties to be used in practical LIHSs. The negative electrodes are insertion-type materials, including carbonaceous materials, layered oxides, spinel oxides, phosphates, fluorophosphates and silicates.[8] The carbonaceous materials used for the cathode in hybrid supercapacitors include graphite,[29] soft carbon,[30] carbon nanotubes (CNTs),[31] AC,[32–36] carbon fibers,[37] 3D porous carbon,[38,39] etc. Other insertion-type negative-electrode materials for LiHSs include LTO and other crystal form of Ti oxides,[12,40–42] spinel-$LiMn_2O_4$ and Ni-doped spinel-$LiMn_2O_4$,[7] Li_2CoPO_4F,[43] $LiSn_2(PO_4)_3$ (LSP),[44] and their composites with carbon[45] or polymer,[46] etc. These insertion-type electrodes can accommodate Li-ions at various potentials. However, the kinetics of Li-intercalation are much lower in comparison to the double-layer formation at the carbonaceous electrode surface. One possible solution to overcome this issue is careful control of the mass ratio between the cathode and anode.[47] Another is to increase the rate capability of the lithium insertion material by properly controlling the particles size and morphology[24] or by introducing very highly conductive carbons materials.[48,49]

REVIEW

3. Graphene-Based LiHSs

Although LIHSs exhibit high energy densities, they usually suffer from poor rate capability and limited long-term cycling stability, due to the poor conductivity of AC and metal oxides, the sluggish Li$^+$ diffusion of metal oxides and graphite materials resulting from the lacking of proper pores, etc. Thus, new electrode materials with both a high SSA and a high conductivity that can meet the requirements for high-performace LIHS applications should be developed.

Graphene has high theoretical surface area and a porous structure, excellent electrical conductivity, high chemical and thermal stability, and high mechanical strength, which make it a competitive candidate for energy-storage applications.[15,50] However, the excellent properties of graphene are based on its nanoscale structure,[51] and bulk graphene always suffer from aggregation and restacking, which result in a much lower SSA than the theoretical value. Much effort has been made to solve this problem, and one of the most effective approaches is to integrate a single graphene sheet into the macroscopic 3D-graphene bulk material, which can also maintain the properties of the monolayer graphene. Thus, one of the current challenges for bulk applications of graphene is how to prepare such graphene-based materials in large quantities and at low cost but retaining the properties of the individual graphene sheets.

Our group has developed a simple method to fabricate a series of 3D-graphene-based bulk materials with graphene nanosheets physically piled up (**Figure 4**b,c).[52] The typical synthesis process (Figure 4a) includes the industry-standard in situ hydrothermal polymerization/carbonization using various cheap biomass (or industry carbon) sources with small amounts of GO to get the hybrid precursor first, and then, via chemical activation (4 M KOH), to obtain the 3D porous graphene-based materials with a high SSA (up to 3300–3523 m^2 g^{-1}) and conductivity (up to 303 S m^{-1}). Figure 4d shows the (PSD) of our porous 3D graphene-based materials. Most of the pores are distributed in the size range from 1 to 10 nm, which is very suitable for the electrolyte to migrate. In contrast, the pore sizes of RP20 (a type of commercial AC) are mainly less than 2 nm. This 3D graphene exhibits both a high specific capacitance/energy and an excellent rate performance for EDLCs. For example, the specific capacitance in the Li-ion electrolyte is in the range from 148 to 187 F g^{-1} at current densities of 5.0 to 0.05 A g^{-1} from 0–2.7 V.

Recent investigations on graphene-based materials for non-aqueous LIHS applications have proved that graphene or RGO can be used as either the positive- or the negative-electrode material in LIHS devices with excellent performance.
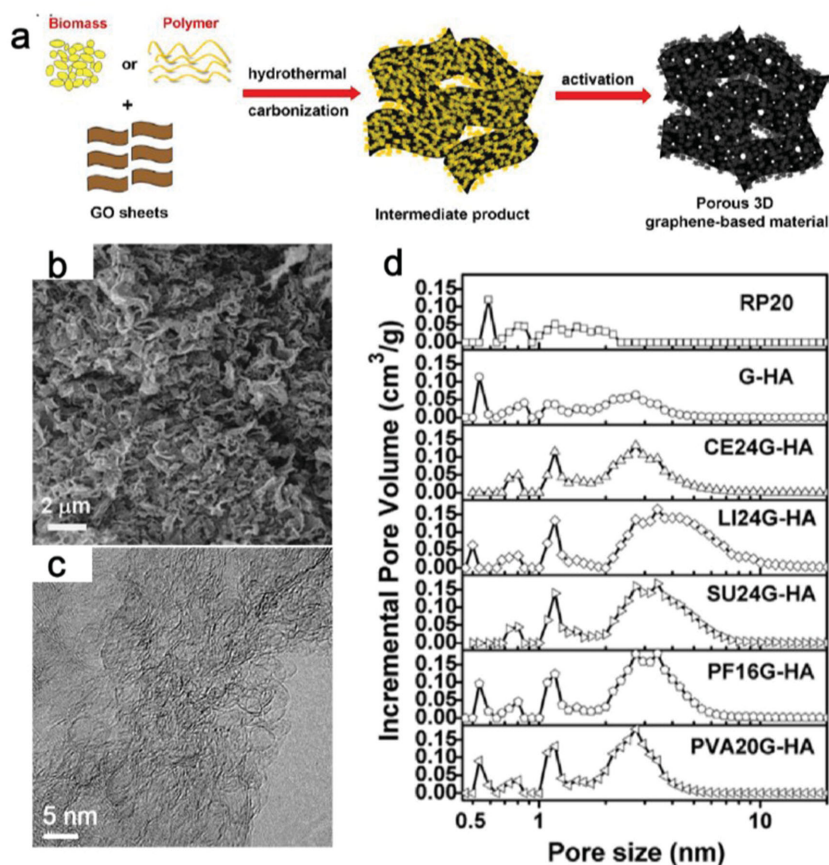
Figure 4. 3D-graphene-based bulk materials. a) A schematic showing the simple and green process of synthesizing porous 3D-graphene-based materials. b,c) SEM (b) and TEM (c) images of 3D-graphene-based material. d) PSD of RP20(a type of AC), G-HA (activated GO) and all the optimized materials. Reproduced with permission.[52] Copyright 2013, Nature Publishing Group.

3.1. Graphene/RGO as Materials for the Positive Electrode

By use of the above-mentioned 3D-graphene bulk material as the positive-electrode material, we designed three types of LIHS systems with either an Fe$_3$O$_4$ nanoparticle/graphene (Fe$_3$O$_4$/G) composite,[53] a graphene-inserted LTO composite (LTO/G),[49] and a flash-reduced GO (FRGO) film[54] as the negative electrode.

In the Fe$_3$O$_4$/G//3D-graphene LIHS device,[53] an Fe$_3$O$_4$ nanoparticle/graphene (Fe$_3$O$_4$/G) composite was prepared by a simple solvothermal approach (**Figure 5**a). This composite exhibited a high reversible specific capacity exceeding 1000 mA h g^{-1} at a current density of 90 mA g^{-1}, along with excellent rate performance and cycle stability. To obtain a high energy density for such an LIHS device, the working potential range and the mass ratio of the electrodes need to be optimized to make full use of the performance of both electrode materials. The voltage window is rather wide, in the range of 1.0–4.0 V, and the best mass ratio of Fe$_3$O$_4$/G: 3D graphene is 4.5:1. Figure 5b shows that both the energy and the power density of this LIHS system were much higher than those of a 3D-graphene symmetric conventional supercapacitor. This LIHS cell exhibited energy
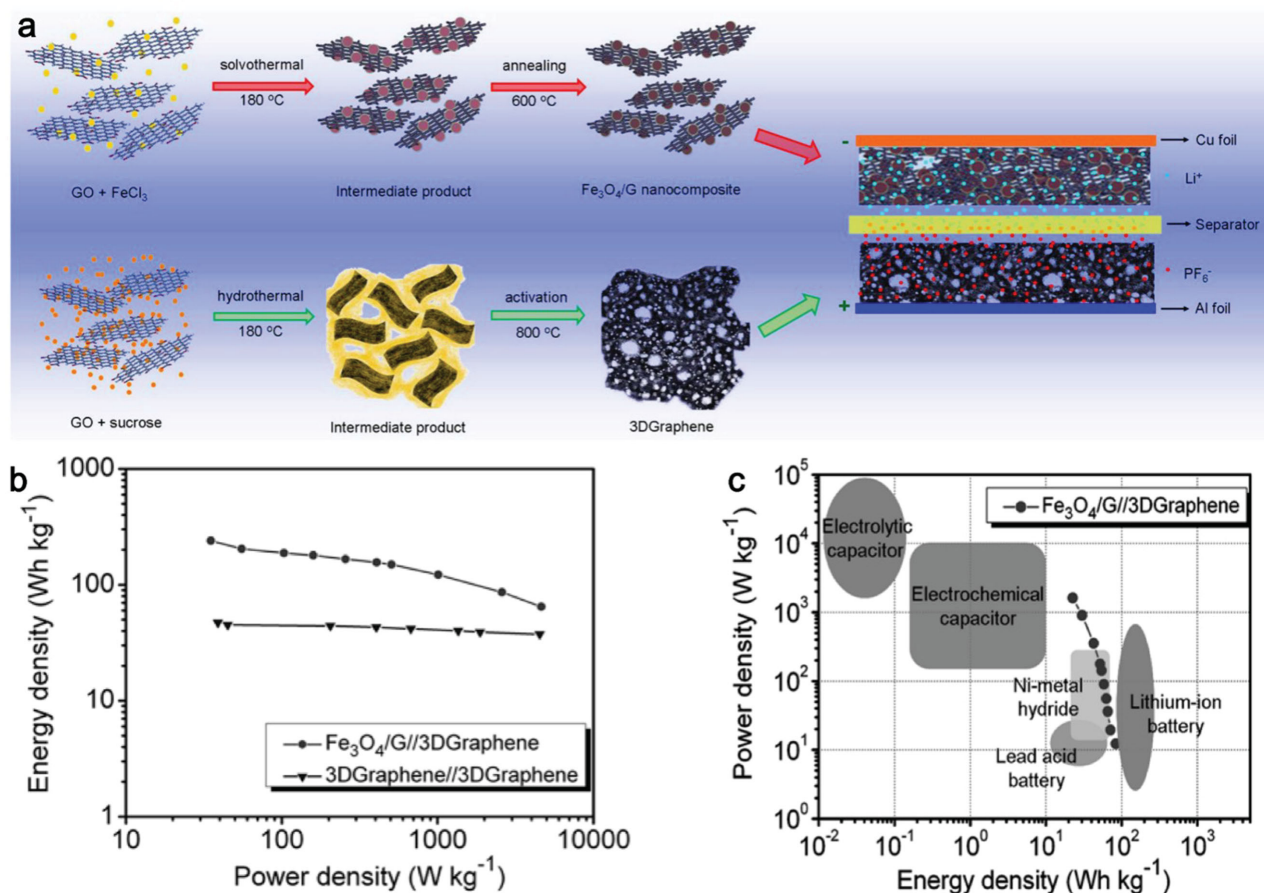
Figure 5. a) Schematic showing the synthesis of the negative-electrode material Fe_3O_4/G nanocomposite and the positive-electrode material 3D graphene, together with the configuration of a Li-ion containing organic hybrid supercapacitor. b) Ragone plots of the Fe_3O_4/G//3D graphene hybrid supercapacitor compared with a 3D graphene//3D graphene3D graphene symmetric supercapacitor at various charge–discharge rates and c) commercial electronic energy-storage devices (all based on total mass of the packaged device). Reproduced with permission.[53] Copyright 2013, The Royal Society of Chemistry.

densities of 204–65 W h kg^{-1} over power densities from 55 to 4600 W kg^{-1}, which are the highest values for LIHSs that have been reported to date. For a packaged cell, this Fe_3O_4/G//3D-graphene LIHS system had a much higher energy density than commercial ECs and it was even comparable with commercial LIBs (Figure 5c).

In the LTO/G//3D-graphene hybrid-supercapacitor system,[49] an LTO/G nanocomposite was fabricated by a process including a solvothermal reaction of an ethanol/water-based colloidal suspension of LTO and GO and subsequent heat treatment (**Figure 6**a). Ball-like LTO particles with a size of 100–500 nm were well dispersed among the crumpled graphene network with a low degree of agglomeration (Figure 6b). The 3D interconnected porous graphene network with its conductive matrices and good mechanical strength and flexibility endowed the composites with larger reversible capacities and enhanced rate capability compared with the theoretical capacity of pure LTO (Figure 6c,d). Compared with the theoretical capacity of 175 mA h g^{-1} for pure LTO, the LTO/G nanocomposite delivered excellent reversible capacities of 207, 190, and 176 mA h g^{-1} at rates of 0.3, 0.5, and 1 C,

respectively, in the potential range 1.0–2.5 V vs Li/Li$^+$, which were among the highest values for LTO-based nanocomposites at the same rates and potential range. The LTO/G//3D graphene LIHS system displayed high energy densities in the range 95–32 W h kg^{-1} in the potential range of 0–3 V over rates from 0.4 to 100 C (where 1 C represents complete discharge in 1 h).

In an FRGO//3D graphene hybrid-supercapacitor system that we described in ref.,[55] the negative-electrode material FRGO (SSA: 277 m^2 g^{-1}) was synthesized by the photoflash reduction of a GO film with simple digital camera flash. The cross-sectional scanning electron microscopy (SEM) images (**Figure 7**a–c) showed large voids and pathways between the highly warped graphene sheets, which should enable rapid and efficient Li-ion shuttling through the graphene sheets. A schematic of the charge/discharge mechanism of our hybrid supercapacitor based on PF16 (a type of 3D graphene) and FRGO is illustrated in Figure 7d. The designed hybrid supercapacitor exhibited high energy densities of 148.3–71.5 W h kg^{-1} with the power densities from 141 to 7800 W kg^{-1} simultaneously. Furthermore, it was also accompanied by good cycle stability. Such
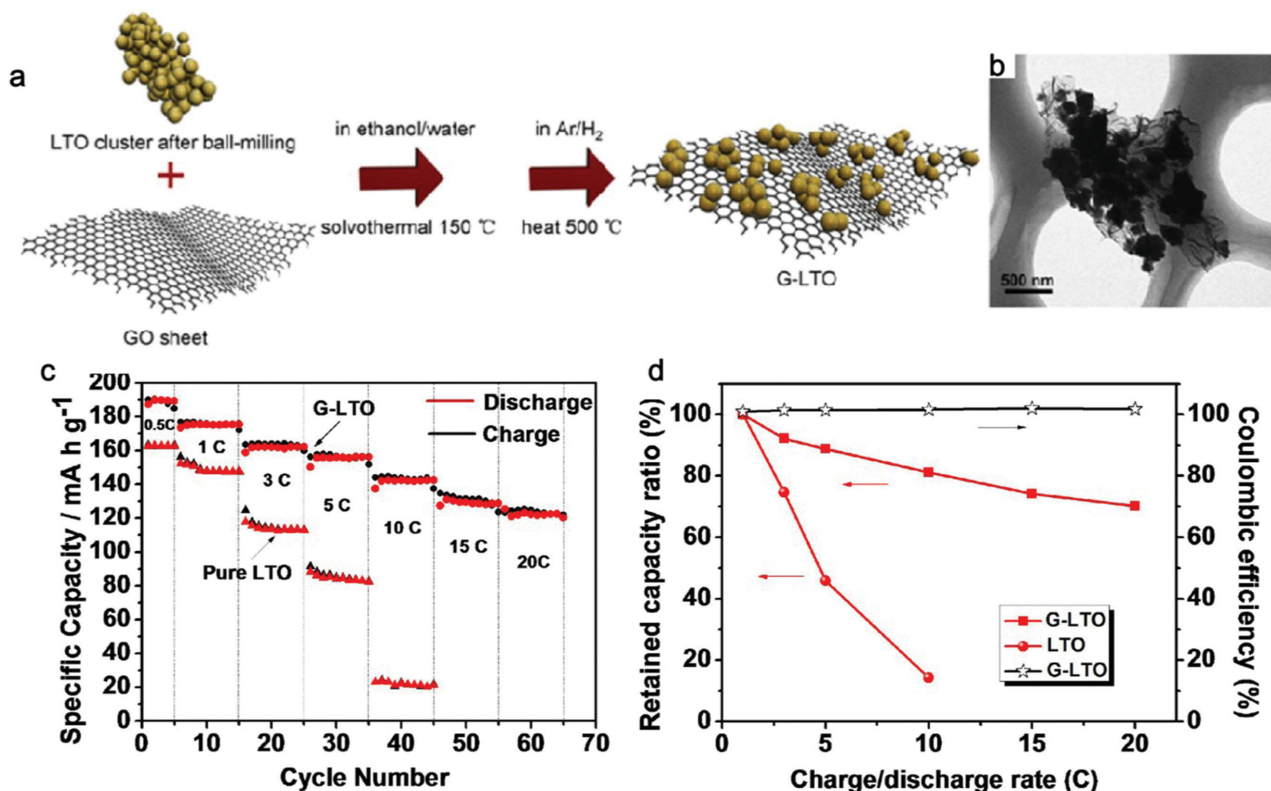
Figure 6. a) Schematic illustration of the synthesis of LTO/graphene (LTO/G) nanocomposite. b) TEM image of the LTO/G nanocomposite. c) The rate capabilities of the LTO/G nanocomposite and pure LTO at different rates. d) Retained discharge-capacity ratio of the LTO/G nanocomposite, pure LTO, and the Coulombic efficiencies at various charge–discharge rates of the LTO/G nanocomposite. Reproduced with permission.[49] Copyright 2013, Springer.

a high performance of all-graphene-based LIHSs is attributed to the usage of superior electrode materials, which takes full advantage of the graphene.

Huang and Yang's groups[54] synthesized a 3D porous graphene macroform (PGM) and utilized it as the positive electrode to construct a high-performance hybrid supercapacitor with an LTO/C hybrid as the negative material (**Figure 8**a). The PGM was synthesized by a hydrothermal process and freeze drying of a graphene oxide (GO) aqueous suspension. The SEM image of the PGM (Figure 8b) displayed a typical 3D continuous network with abundant micro-, meso-, and macropores. The SSA of the PGM was determined to be 373 $m^2 g^{-1}$. The optimized mass ratio of the PGM:LTO/C was 2:1. The hybrid supercapacitor delivered a maximum energy density of 72 W h kg^{-1} at 650 W kg^{-1} in a voltage range of 1–3 V, and it can still offer an energy density of 40 W h kg^{-1} with a power density of 8.3 kW kg^{-1}. Furthermore, the LIHS exhibited a stable energy-density retention of 65% for 1000 cycles at an extremely high current density of 10 A g^{-1}.

The excellent performance of the above graphene-based hybrid supercapacitor indicates that 3D graphene, with its interconnected conductive network, high surface area, and microporous and mesoporous structure, may have great potential as the positive-electrode material in LiHS applications.

3.2. Graphene/RGO as Materials for Negative Electrodes

The early application of graphene material as the negative electrode for LiHSs in aqueous systems was investigated by Liu's group[56] in 2011. The graphene material they used was RGO, which was prepared by the reduction of GO with a hydrazine solution and followed by heating to 95 °C. The anode material was a graphene–manganese oxide hybrid material (MnO_2/G), which was obtained by solution-phase assembly of aqueous dispersions of graphene nanosheets and MnO_2 nanosheets at room temperature. The electrolyte used was a 1 M Na_2SO_4 solution. The stable electrochemical window was estimated before cycling the hybrid cell. The potential of the asymmetric unit cell could reach 1.7 V in the fully charged state. This LIHS exhibited an energy density of 10.03 W h kg^{-1} at an average power density of 2.53 kW kg^{-1}, and the capacitance retention of hybrid supercapacitor was 69% at the constant current density of 2230 mA g^{-1} after repeating for 10 000 cycles.

In 2012, Ruoff's group[57] used an activated graphene with a high surface area and high porosity as the cathode material for hybrid supercapacitors in a non-aqueous system. This activated graphene was produced firstly by irradiating the GO in a microwave oven to prepare microwave-exfoliated graphite oxide (MEGO), and then the as-prepared MEGO powder was dispersed and soaked in aqueous KOH solution followed by
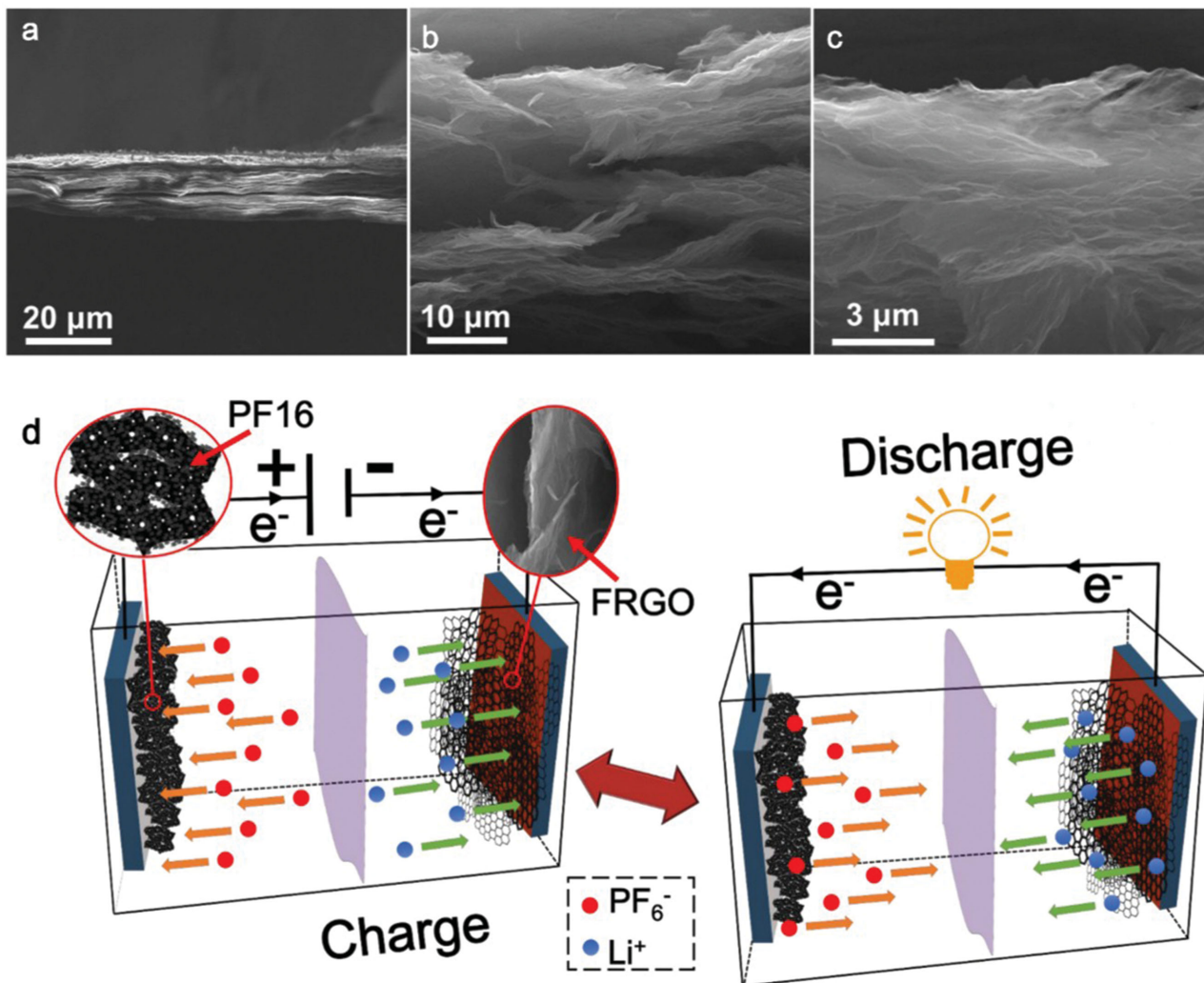
Figure 7. a–c) SEM images of the side view of FRGO film. d) Schematic of the charge/discharge mechanism of an LIHS based on PF16 (a 3D graphene) and FRGO. Reproduced with permission.[55] Copyright 2013, Elsevier.

filtration and drying to form the MEGO/KOH mixture. Finally, the MEGO/KOH mixture was put into a tube furnace under flowing argon at a certain pressure and heated at 800 °C for 1 h to obtain the a-MEGO. This material had a continuous network of pores of extremely small sizes ranging from 0.1 to 10 nm and a very high specific surface area of 3100 m^2 g^{-1}. The LIHS system was constructed with a-MEGO as the cathode and with either graphite or LTO for the anode materials. For an a-MEGO/graphite hybrid cell, the specific capacitance was as high as 266 F g^{-1} for the active materials at operating potentials of 4 V, yielding gravimetric energy densities for a packaged cell of 53.2 W h kg^{-1}.

Choi's group[58] considered that the small capacities of activated carbon cathodes limited the energy density of conventional non-aqueous LIHSs, so they used urea-reduced graphene instead of AC to overcome this limitation. The results showed that the amide functional groups on graphene resulting from the urea reduction favored reversible Li binding, and the specific capacity improved 37% compared with an AC-based device.

Ogale's group[59] reported the preparation and application of a 3D-graphene-based porous carbon for LiHSs. This material had a 3D n-graphene cage morphology produced by the pyrolysis of a tailored oligomer. It evolved through the self-assembly of the porous graphene network. The specific functional groups (ACOONa) of the oligomer were derived from 4-amino benzoic acid and rendered a molecular-level activation without any external activating agent. This oligomer-derived carbon (ODC) exhibited an efficient performance for LIHSs owing to its high surface area, 3D interconnectivity, and the appropriate pore-size distribution. This ODC//LTO LIHS system delivered a maximum energy density of ca. 63 W h kg^{-1}. This work opened up an avenue for the preparation of 3D architectures of high-surface-area porous graphene based on polymer precursors. Earlier, Ogale and co-workers had used trigol-reduced GO as the negative electrode and LTO as the positive electrode to construct a LIHS,[60] which delivered exceptional cyclability for about 5000 cycles with a maximum deliverable energy density of ca. 45 W h kg^{-1}.
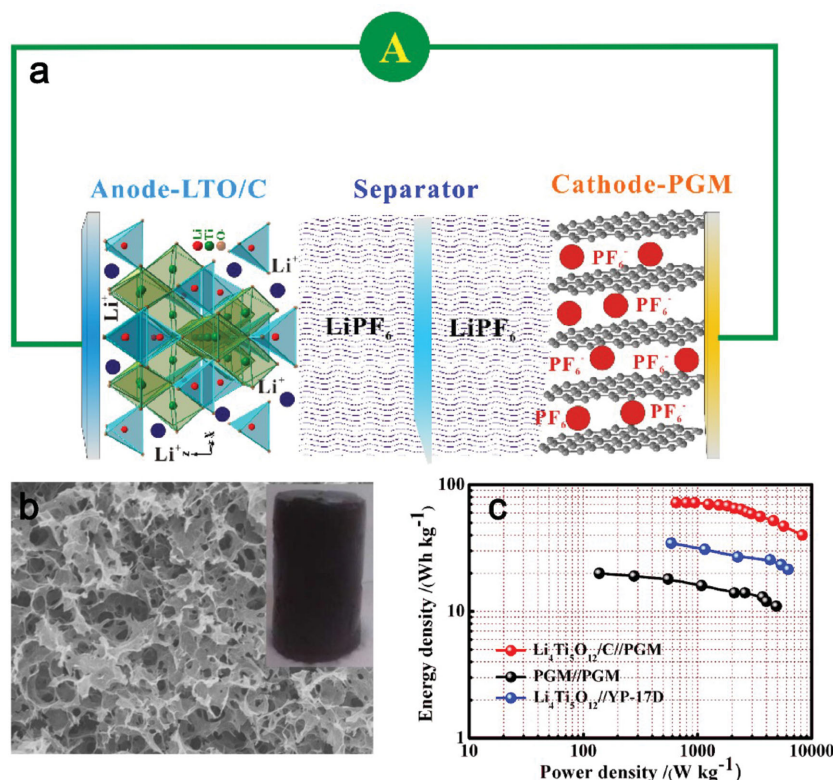
Figure 8. a) Illustration of the LIC in which a porous graphene macroform (PGM) and an LTO/C hybrid are used as the positive and negative electrodes, respectively. b) SEM of the PGM. The inset shows the corresponding picture. c) Ragone plots of the LTO/C//PGM LIC, PGM//PGM SC, and LTO//YP-17D LICs. All the values of power and energy density are based on the active materials. Reproduced with permission.[54] Copyright 2015, Elsevier.

Zhou's group[61] utilized pre-lithiated graphene nanosheets as the negative electrode material for an LIHS and compared them with graphite. Pre-lithiated carbon materials could provide low potentials to negative electrodes and increase the open-circuit voltage (V_{OC}), and thus enhanced the energy density of the hybrid supercapacitor accordingly. The LIHS system showed a specific capacitance of 168.5 F g^{-1} with 74% capacitance retention at 400 mA g^{-1} after 300 cycles. Moreover, the capacitors delivered a maximum power density of 222.2 W kg^{-1} at an energy density of 61.7 W h kg^{-1}, when operated in the voltage range of 2.0–4.0 V. Compared with pre-lithiated graphite, the graphene-based hybrid supercapacitor system showed a better electrochemical performance, which could be attributed to the microstructure consisting of crosslinked graphene nanosheets with high specific surface areas and rich pores. This result indicated that the proposed pre-lithiated graphene nanosheets are a promising negative-electrode material for high-power hybrid supercapacitors.

Wang et al.[62] used a 3D-graphene hydrogel as the negative electrode, coupled with a TiO$_2$-nanobelt-array positive electrode to construct a non-aqueous LIHS system. A high energy density of 82 W h kg^{-1} was achieved at a power density of 570 W kg^{-1}. Even at an 8.4 s charge/discharge rate, an energy density as high as 21 W h kg^{-1} could be retained.

It is noteworthy that, as a lithium-intercalated negative material, having an appropriate pore structure is very important, as it

can enable the rapid and efficient Li-ion shuttling through the graphene sheets, and thus impart a high electrochemical performance.

4. Graphene/RGO as a Conductive Additive for LIHSs

Graphene has been combined with low-conductivity materials such as LTO,[63,49] Nb$_2$O$_5$,[64] TiN,[65] CuO,[66] MnFe$_2$O$_4$,[67] and MoO$_2$,[68] to aid charge transfer and promote high-rate charge–discharge cycles. These composites can serve as either positive- or negative-electrode materials.

Kim et al.[63] reported a hybrid supercapacitor employing RGO-wrapped LTO as the anode. They believed that wrapping the LTO particles with graphene helped to remedy the intrinsically low electronic conductivity of the LTO and dramatically improved the rate capability. This LTO/RGO//AC hybrid supercapacitor delivered a specific energy of up to 50 W kg^{-1} and could maintain near 15 W h kg^{-1}. Xu and co-workers reported[64] is by a binder-free Nb$_2$O$_5$/graphene composite used as the anode, coupled with an AC cathode for a hybrid supercapacitor, and found that the existence of a highly conductive graphene support could enhance the rate capability. A Nb$_2$O$_5$/graphene composite was obtained by the electrostatic deposition of hydrothermally prepared Nb$_2$O$_5$ particles onto graphene oxide and followed by thermal reduction. This composite exhibited enhanced cyclability with a capacity retention of 91.2%, compared with the 74.4% of the pure Nb$_2$O$_5$ half-cell when tested at a rate of 2000 mA g^{-1} (10 C). As a result, the hybrid supercapacitor system delivered a maximum energy and power density of 29 W h kg^{-1} and 2.9 kW kg^{-1}.

Similar results have also been reported in other graphene/metal oxide composites,[64–67] and the enhancement in the electrochemical properties was attributed to the introduction of graphene, which not only constructs 2D or 3D conductive networks, but also disperses and confines the metal oxide nanocrystals. Sometimes, the synergistic effect of graphene with metal oxide further contributes to the performance of the composite.

Ternary composites have also attracted much attention due to their multifunctional properties. Selvan's group[67] reported the preparation of a MnFe$_2$O$_4$/graphene/polyaniline (PAN) ternary composite and used it as the cathode for hybrid supercapacitors. The typical synthesis method of this ternary hybrid composite was the in situ chemical oxidative polymerization of aniline with hydrothermally synthesized MnFe$_2$O$_4$ and NaOH-reduced graphene. The sizes of the obtained MnFe$_2$O$_4$ particles were in the range of 75–100 nm. The ternary composite exhibited a specific capacitance of 338 F g^{-1} at 0.5 mA cm^{-2} in 1 M NaCl aqueous electrolyte, which was 10 times greater than that of the pristine MnFe$_2$O$_4$. A hybrid supercapacitor with AC as
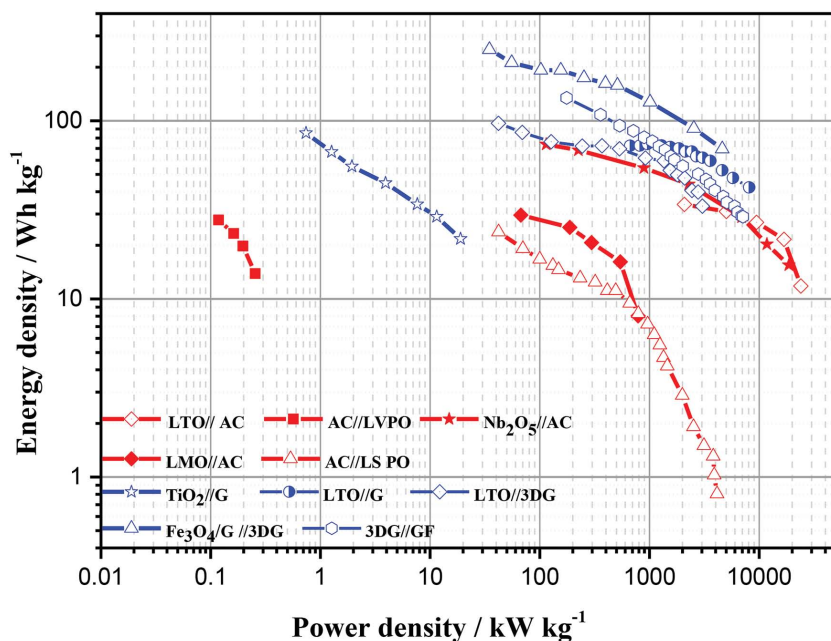
Figure 9. Left) The Ragone plot of an LIC device based on AC (red line) and a graphene electrode (blue line). The abbreviations represent: LTO: $Li_4Ti_5O_{12}$, LVPO: $Li_3V_2(PO_4)_3$, LMO: $LiMn_2O_4$, LSPO: $LiSn_2(PO_4)_3$. The LMO//AC is an aqueous LIHS system.[69] The others are non-aqueous systems. (LTO//AC: ref.[47]; AC//LVPO: ref.[32]; Nb_2O_5//AC: ref.[70]; AC//LS PO: ref.[44]; TiO_2//G: ref.[62]; LTO//G: ref.[54]; LTO//3DG: ref.[49]; Fe_3O_4/G //3DG: ref.[53]; 3DG//GF: ref.[55])

the anode provided a specific capacitance of about 51.87 F g^{-1} at 5 mV s^{-1} and its energy density was 10.25 W h kg^{-1} at 10 mA cm^{-2}. The excellent electrochemical performance of the ternary composite was due to the synergistic effect of these components.

5. Discussion

Figure 9 shows the Ragone plot of several typical AC- and graphene-based LIHS systems.

It can be seen that 3D-graphene-based LIHSs show similar a level of power density, but a higher energy density than the AC electrode. As the most intensively investigated and commercially used carbonaceous material for energy-storage applications, activated carbons have many advantages, including high surface area, good chemical stability, long-term cyclability, and low cost. However, their practical applications are still limited to some extent as the energy density is still relatively low and the control of the pore-size distribution (PSD) and pore structure is still a challenge. Most of the pores' sizes of commercial AC are usually less than 2 nm with quantities of small pores (< 0.6 nm), which prevents the entry of organic electrolyte ions (>1 nm) and hydrate ions (typically range in the size 0.6–0.8 nm).[13] Graphene has a high theoretical SSA and a high conductivity. Though bulk graphene materials suffer from aggregation and restacking, physical and chemical activation or construction a 3D-graphene framework by physical or chemical bonding can highly improve this problem. For example, through microwave-treatment and chemical activation, a graphene material

with small pore sizes ranging from 0.1 to 10 nm and a high SSA of 3100 m^2 g^{-1} was obtained.[57] By in situ hydrothermal polymerization/carbonization of industry-carbon sources with small amounts of GO, followed by chemical activation, a 3D porous graphene-based material with a high SSA (up to 3300–3523 m^2 g^{-1}) and conductivity (up to 303 S m^{-1}) was fabricated.[52] Compared with AC, graphene has a mesoporous structure, which enables the ions to shuttle through easily, as well as a high conductivity so as to decrease the internal resistance and be beneficial for the transport of electrons. Furthermore, oxygen-containing groups on the surface of the graphene lead to a good wettability between the electrode material and the electrolyte. Thus, 3D-graphene-based LIHSs may show a better performance than AC-based devices.

Figure 10 shows the Ragone plot of various insertion-type positive-electrode materials tested for LIHS applications in non-aqueous media.[8] Compared with the performance of 3D-graphene-anode-based LIHS systems, it is obviously that the 3D-graphene-anode-based LIHS systems show similar or even higher energy density, but a much higher power density than insertion-type anodes. The insertion-type negative-electrode materials show a similar performance to the anode.[8] This poor rate capability and cyclability is mainly because of the poor conductivity of these insertion-type materials and the sluggish Li$^+$ diffusion that results from the lack of appropriately sized pores. Thus, to improve their performance, making composites from materials with
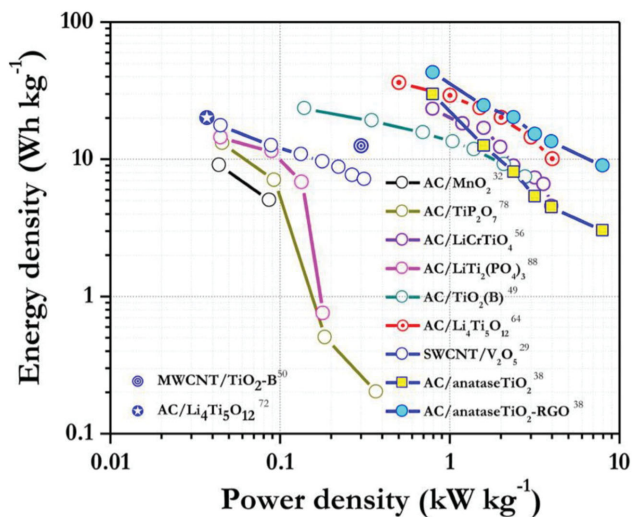
Figure 10. The Ragone plot indicating the performance of various insertion-type anode materials tested for LIHS applications in non-aqueous media. Reproduced with permission.[8] Copyright 2014, American Chemical Society. The reference citations in the legend in the figure refer to the reference numbers in the article in ref.[8]
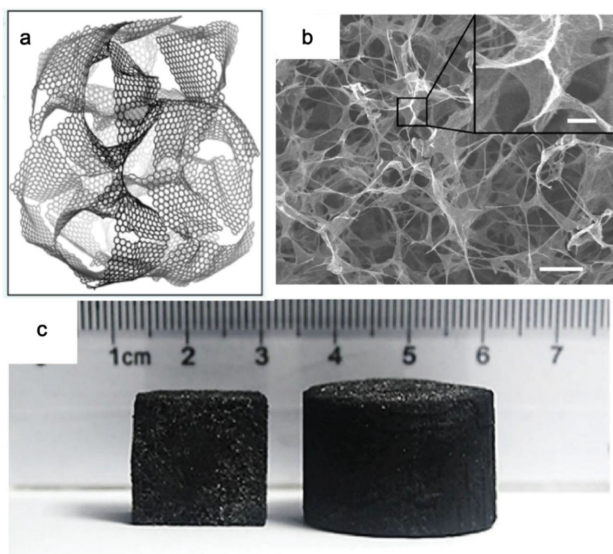
Figure 11. Graphene sponge via chemical bonding. a) The proposed 3D-structure model of the graphene sponge. b) Radial cross-sectional SEM image of a graphene sponge (scale bar, 20 μm) and a magnified SEM image (inset, scale bar, 5 μm) showing the interwall connection. c) Photographs of rectangular (left) and cylindrical (right) graphene sponges. Reproduced with permission.[18] Copyright 2015, Nature Publishing Group.

high conductivity and a mesoporous structure, such as 3D graphene, is a promising approach.

From the above analysis, it can be seen that 3D graphene is a very attractive material for LIHS applications. Thus, one of the current challenges is how to prepare such 3D-graphene-based materials in large quantities and at low cost, but retaining the properties of the individual graphene sheet.

The hydrothermal process is an effective approach to obtain 3D graphene. Many pieces of work have been reported.[17,71,72] Recently, our group fabricated a chemically bonded 3D-graphene material, (**Figure 11**) a unique bulk and monolithic-graphene-based sponge, by a modified solvothermal reaction of GO sheets in alcohol and a subsequent thermal-annealing process.[18] The network was formed by the crosslinking of the oxygen-containing groups on the surface of the graphene sheets. Under the solvothermal conditions, reactions are expected between/among the OH, COOH and epoxy bond functional groups of adjacent graphene sheets to generate aromatic ether and ester bonds between the sheets. This type of graphene sponge has a low density, varying from 0.3 to 14 mg cm^{-3} by varying the GO concentrations. It demonstrates highly repeatable compression and displays Poisson's ratios in all directions that are near-zero. Furthermore, its reversible rubber-like compressive elasticity can be observed even in liquid nitrogen (−196 °C) and at temperatures as high as 900 °C. Even when the maximum (>99%) strain was applied, the graphene sponge exhibited highly repeatable compression reversibility. These extraordinary compressive properties and air-like density make it an ideal material for application in flexible and wearable energy devices. Its excellent performance is mainly due to the chemically bonded 3D structure. However, the size of the

3D graphene is limited by the size of the Teflon-lined autoclave used in its production.

Cheng's group prepared an interconnected 3D graphene foam by chemical vapor deposition (CVD) with high electrical conductivity and a low number of defects.[19] However, as the graphene foam inherits the structure of the nickel-foam template, which has a pore size usually of hundreds of micrometers, the obtained graphene foam possessed large pore sizes with high porosity (about 99.7%), which cannot meet the demands of a good electrode material (pore size 1.0–10 nm). Thus, a new template with a mesoporous structure should be used to grow of 3D graphene with an appropriate structure. Also, the strong hydrophobic property of this 3D graphene limited its application.[73]

6. Conclusion and Outlook

The construction of lithium-ion hybrid supercapacitors (LiHSs) has been proven to be an effective way to enhance the electrochemical performance of supercapacitors for a combination of the rapid charge–discharge and long cycle life of supercapacitors with the high energy-storage capacity of lithium-ion batteries. However, the full potential of LiHSs for high-performance energy systems has not yet been realized. Nowadays, LiHSs still face many challenges, such as poor rate capability and limited long-term cycling stability, due to the poor conductivity of AC and metal oxides, and the sluggish Li$^+$ diffusion of metal oxides and graphite materials resulting from the lacking of proper pores, etc. 3D-graphene-based materials possess high specific surface area, a suitable tunable mesoporous structure, and a high conductivity, which makes them a good candidate for next-generation electrode materials for LiHSs. Therefore, a promising strategy for improving the performance of LiHSs is the fabrication of graphene-based 3D carbon materials (graphene only or graphene/AC composites) for EDLC-type electrodes, while synthesizing 3D open frameworks of composites of graphene with intercalation materials for battery-type electrodes. Hydrothermal synthesis and CVD growth are two effective methods for the fabrication of 3D graphene, but both have their limitations. Thus, one of the current challenges is how to prepare such 3D-graphene material on a large scale and at low cost. Moreover, much work must be done to study the interaction between graphene and oxides/intercalation compounds, which will help in understanding the synergistic effects of graphene-based 3D composites. Furthermore, using an aqueous electrolyte instead of a commercially used organic electrolyte may have some advantages. Though aqueous electrolytes have a narrow electrochemical window, which is unfavorable for energy storage, its high ionic conductivity is favorable for improving the power density. Moreover, aqueous electrolytes possess the merits of low cost, higher safety, and environment-friendliness.

With the development of graphene-based materials, especially the 3D graphene framework via chemical bonding, and the investigation more deeply and thoroughly, we believe LiHSs will become the ultimate power source for hybrid and all-electric vehicles in the near future. One important issue for such applications with graphene is to prepare the bulk

Materials
Views
www.MaterialsViews.com

ADVANCED
MATERIALS
www.advmat.de

REVIEW

graphene-based electrode materials on both a large scale and at lost cost, and that they are also compatible with the current supercapacitor and lithium-battery technology platforms.

Acknowledgements

[1] J. Yan, Q. Wang, T. Wei, Z. Fan, *Adv. Energy Mater.* **2014**, *4*, 1300816.
[2] Y. Huang, J. Liang, Y. Chen, *Small* **2012**, *8*, 1805.
[3] Y. Zhai, Y. Dou, D. Zhao, P. F. Fulvio, R. T. Mayes, S. Dai, *Adv. Mater.* **2011**, *23*, 4828.
[4] Y. Gogotsi, P. Simon, *Science* **2011**, *334*, 917.
[5] A. S. Aricò, P. Bruce, B. Scrosati, J.-M. Tarascon, W. Van Schalkwijk, *Nat. Mater.* **2005**, *4*, 366.
[6] D. P. Dubal, O. Ayyad, V. Ruiz, P. Gómez-Romero, *Chem. Soc. Rev.* **2015**, *44*, 1777.
[7] K. Naoi, S. Ishimoto, J.-i. Miyamoto, W. Naoi, *Energy Environ. Sci.* **2012**, *5*, 9363.
[8] V. Aravindan, J. Gnanaraj, Y.-S. Lee, S. Madhavi, *Chem. Rev.* **2014**, *114*, 11619.
[9] F. X. Wang, S. Y. Xiao, Y. Y. Hou, C. L. Hu, L. L. Liu, Y. P. Wu, *RSC Adv.* **2013**, *3*, 13059.
[10] S. Faraji, F. N. Ani, *Renewable Sustainable Energy Rev.* **2015**, *42*, 823.
[11] L. G. H. Staaf, P. Lundgren, P. Enoksson, *Nano Energy* **2014**, *9*, 128.
[12] Y. B. Tan, J. M. Lee, *J. Mater. Chem. A.* **2013**, *1*, 14814.
[13] M. Sevilla, R. Mokaya, *Energy Environ. Sci.* **2014**, *7*, 1250.
[14] D. Cericola, R. Kötz, *Electrochim. Acta.* **2012**, *72*, 1.
[15] F. Bonaccorso, L. Colombo, G. Yu, M. Stoller, V. Tozzini, A. C. Ferrari, R. S. Ruoff, V. Pellegrini, *Science* **2015**, *347*, 1246501.
[16] J. Liu, *Nat. Nanotechnol.* **2014**, *9*, 739.
[17] Y. Ma, Y. Chen, *Natl. Sci. Rev.* **2015**, *2*, 40.
[18] Y. Wu, N. Yi, L. Huang, T. Zhang, S. Fang, H. Chang, N. Li, J. Oh, J. A. Lee, M. Kozlov, A. Chipara, H. Terrones, P. Xiao, G. Long, Y. Huang, F. Zhang, L. Zhang, X. Lepro, C. Haines, M. Lima, N. Lopez, L. Rajukumar, A. Elias, S. Feng, S. Kim, N. Narayanan, P. Ajayan, M. Terrones, A. Aliev, P. Chu, Z. Zhang, R. Baughman, Y. Chen, *Nat. Commun.* **2015**, *6*, 6141.
[19] Z. Chen, W. Ren, L. Gao, B. Liu, S. Pei, H.-M. Cheng, *Nat. Mater.* **2011**, *10*, 424.
[20] H. Kim, K. Y. Park, M. Y. Cho, M. H. Kim, J. Hong, S. K. Jung, K. C. Roh, K. Kang, *ChemElectroChem* **2014**, *1*, 125.
[21] L. Zhang, X. Zhang, F. Zhang, G. Long, T. Zhang, K. Leng, Y. Zhang, Y. Huang, Y. Ma, M. Zhang, *J. Am. Chem. Soc.* **2013**, *135*, 5921.
[22] I. Plitz, A. DuPasquier, F. Badway, J. Gural, N. Pereira, A. Gmitter, G. Amatucci, *Appl. Phys. A: Mater. Sci. Process.* **2006**, *82*, 615.
[23] M. Chiku, M. Toda, E. Higuchi, H. Inoue, *J. Power Sources* **2015**, *286*, 193.
[24] H. Inoue, Y. Namba, E. Higuchi, *J. Power Sources* **2010**, *195*, 6239.
[25] M. Chiku, M. Toda, E. Higuchi, C. B. Tsai, P. Chen, W. Ho, H. Inoue, *ECS Trans.* **2013**, *50*, 103.
[26] A. Yuan, X. Wang, Y. Wang, J. Hu, *Energy Convers. Manage.* **2010**, *51*, 2588.

[27] Q. Qu, Y. Shi, L. Li, W. Guo, Y. Wu, H. Zhang, S. Guan, R. Holze, *Electrochem. Commun.* **2009**, *11*, 1325.
[28] X. Du, C. Wang, M. Chen, Y. Jiao, J. Wang, *J. Phys. Chem. C* **2009**, *113*, 2643.
[29] S. Li, X. Wang, *J. Power Sources* **2015**, *282*, 394.
[30] M. Schroeder, S. Menne, J. Ségalini, D. Saurel, M. Casas-Cabanas, S. Passerini, M. Winter, A. Balducci, *J. Power Sources* **2014**, *266*, 250.
[31] Q. Wang, Z. Wen, J. Li, *Adv. Funct. Mater.* **2006**, *16*, 2141.
[32] R. Satish, V. Aravindan, W. C. Ling, S. Madhavi, *J. Power Sources* **2015**, *281*, 310.
[33] N. Arun, A. Jain, V. Aravindan, S. Jayaraman, W. Ling, M. Srinivasan, S. Madhavi, *Nano Energy* **2015**, *12*, 69.
[34] S. Amaresh, K. Karthikeyan, I. Jang, Y. Lee, *J. Mater. Chem. A* **2014**, *2*, 11099.
[35] W. Cao, Y. Li, B. Fitch, J. Shih, T. Doung, J. Zheng, *J. Power Sources* **2014**, *268*, 841.
[36] W. Cao, M. Greenleaf, Y. Li, D. Adams, M. Hagen, T. Doung, J. Zheng, *J. Power Sources* **2015**, *280*, 600.
[37] K. Kaliyappan, S. Amaresh, Y.-S. Lee, *ACS Appl. Mater. Interfaces* **2014**, *6*, 11357.
[38] A. Banerjee, K. K. Upadhyay, D. Puthusseri, V. Aravindan, S. Madhavi, S. Ogale, *Nanoscale* **2014**, *6*, 4387.
[39] D. Puthusseri, V. Aravindan, S. Madhavi, S. Ogale, *Electrochim. Acta* **2014**, *130*, 766.
[40] G. G. Amatucci, F. Badway, A. Du Pasquier, T. Zheng, *J. Electrochem. Soc.* **2001**, *148*, A930.
[41] V. Aravindan, N. Shubha, W. C. Ling, S. Madhavi, *J. Mater. Chem. A* **2013**, *1*, 6145.
[42] C.-J. Peng, D.-S. Tsai, C.-H. Chang, H.-Y. Wei, *J. Power Sources* **2015**, *274*, 15.
[43] K. Karthikeyan, S. Amaresh, K. Kim, S. Kim, K. Chung, B. Cho, Y. Lee, *Nanoscale* **2013**, *5*, 5958.
[44] C. Peng, D. Tsai, C. Chang, M. Le, *J. Alloys. Compd.* **2015**, *627*, 186.
[45] X. Sun, X. Zhang, H. Zhang, N. Xu, K. Wang, Y. Ma, *J. Power Sources* **2014**, *270*, 318.
[46] K. Karthikeyan, S. Amaresh, V. Aravindan, H. Kim, K. Kang, Y. Lee, *J. Mater. Chem. A* **2012**, *1*, 707.
[47] S. Dsoke, B. Fuchs, E. Gucciardi, M. Wohlfahrt-Mehrens, *J. Power Sources* **2015**, *282*, 385.
[48] N. Katsuhiko, N. Wako, *Boletín Grupo Español Carbón* **2013**, *28*, 2.
[49] K. Leng, F. Zhang, L. Zhang, T. Zhang, Y. Wu, Y. Lu, Y. Huang, Y. Chen, *Nano. Res.* **2013**, *6*, 581.
[50] L. Wen, C. Liu, R. Song, H. Luo, Y. Shi, F. Li, H. Cheng, *Acta Chim. Sin.* **2014**, *72*, 333.
[51] M. Zeng, W. L. Wang, X. D. Bai, *Chin. Phys. B* **2013**, *22*, 8.
[52] L. Zhang, F. Zhang, X. Yang, G. Long, Y. Wu, T. Zhang, K. Leng, Y. Huang, Y. Ma, A. Yu, *Sci. Rep.* **2013**, *3*, 1408.
[53] F. Zhang, T. Zhang, X. Yang, L. Zhang, K. Leng, Y. Huang, Y. Chen, *Energy Environ. Sci.* **2013**, *6*, 1623.
[54] L. Ye, Q. Liang, Y. Lei, X. Yu, C. Han, W. Shen, Z. Huang, F. Kang, Q. Yang, *J. Power Sources* **2015**, *282*, 174.
[55] T. Zhang, F. Zhang, L. Zhang, Y. Lu, Y. Zhang, X. Yang, Y. Ma, Y. Huang, *Carbon* **2015**, *92*, 106.
[56] L. Deng, G. Zhu, J. Wang, L. Kang, Z. Liu, Z. Yang, Z. Wang, *J. Power Sources* **2011**, *196*, 10782.
[57] M. Stoller, S. Murali, N. Quarles, Y. Zhu, J. Potts, X. Zhu, H. Ha, R. Ruoff, *Phys. Chem. Chem. Phys.* **2012**, *14*, 3388.
[58] J. Lee, W. Shin, M. Ryou, J. Jin, J. Kim, J. Choi, *ChemSusChem* **2012**, *5*, 2328.
[59] R. Gokhale, V. Aravindan, P. Yadav, S. Jain, D. Phase, S. Madhavi, S. Ogale, *Carbon* **2014**, *80*, 462.
[60] V. Aravindan, D. Mhamane, W. Ling, S. Ogale, S. Madhavi, *ChemSusChem* **2013**, *6*, 2240.

REVIEW

[61] J. Ren, L. Su, X. Qin, M. Yang, J. Wei, Z. Zhou, P. Shen, *J. Power Sources* **2014**, *264*, 108.

[62] H. Wang, C. Guan, X. Wang, H. Fan, *Small* **2015**, *11*, 1470.

[63] H. Kim, M. Y. Cho, M. H. Kim, K. Y. Park, H. Gwon, Y. Lee, K. C. Roh, K. Kang, *Adv. Energy Mater.* **2013**, *3*, 1500.

[64] L. P. Wang, L. Yu, R. Satish, J. Zhu, Q. Yan, M. Srinivasan, Z. Xu, *RSC. Adv.* **2014**, *4*, 37389.

[65] P. Han, Y. Yue, X. Wang, W. Ma, S. Dong, K. Zhang, C. Zhang, G. Cui, *J. Mater. Chem.* **2012**, *22*, 24918.

[66] K. Purushothaman, B. Saravanakumar, I. Babu, B. Sethuraman, G. Muralidharan, *RSC. Adv.* **2014**, *4*, 23485.

[67] K. V. Sankar, R. K. Selvan, *RSC. Adv.* **2014**, *4*, 17555.

[68] P. Han, W. Ma, S. Pang, Q. Kong, J. Yao, C. Bi, G. Cui, *J. Mater. Chem. A* **2013**, *1*, 5949.

[69] C. Rong, S. Chen, J. Han, K. Zhang, D. Wang, X. Mi, X. Wei, *J. Renewable Sustainable Energy* **2015**, *7*, 023104.

[70] E. Lim, H Kim, C. Jo, J. Chun, K. Ku, S. Kim, H. Lee, I. Nam, S. Yoon, K. Kang, J. Lee, *ACS Nano* **2014**, *8*, 8968.

[71] H. Bi, K. Yin, X. Xie, Y. Zhou, N. Wan, F. Xu, F. Banhart, L. Sun, R. S. Ruoff, *Adv. Mater.* **2012**, *24*, 5124.

[72] Y. Xu, K. Sheng, C. Li, G. Shi, *ACS Nano* **2010**, *4*, 4324.

[73] S. He, W. Chen, *Nanoscale* **2015**, *7*, 6957.